Science and Technology of Advanced Materials

ISSN: (Print) (Online) Journal homepage: www.tandfonline.com/journals/tsta20

Epitaxial lateral overgrowth of *m*-plane α-Ga_2O_3 by halide vapor phase epitaxy

Yuichi Oshima & Takashi Shinohe

To cite this article: Yuichi Oshima & Takashi Shinohe (2025) Epitaxial lateral overgrowth of *m*-plane α-Ga_2O_3 by halide vapor phase epitaxy, Science and Technology of Advanced Materials, 26:1, 2485869, DOI: 10.1080/14686996.2025.2485869

To link to this article: https://doi.org/10.1080/14686996.2025.2485869

© 2025 The Author(s). Published by National Institute for Materials Science in partnership with Taylor & Francis Group.

Published online: 22 Apr 2025.

Submit your article to this journal

Article views: 238

View related articles

View Crossmark data

Full Terms & Conditions of access and use can be found at https://www.tandfonline.com/action/journalInformation?journalCode=tsta20

SCIENCE AND TECHNOLOGY OF ADVANCED MATERIALS
2025, VOL. 26, NO. 1, 2485869
https://doi.org/10.1080/14686996.2025.2485869

Epitaxial lateral overgrowth of *m*-plane α-Ga_2O_3 by halide vapor phase epitaxy

Yuichi Oshima [a] and Takashi Shinohe [b]

[a]Research Center for Electronic and Optical Materials, National Institute for Materials Science, Tsukuba, Japan;
[b]FLOSFIA, Inc, Kyoto, Japan

ABSTRACT
We demonstrated the epitaxial lateral overgrowth of *m*-plane α-Ga_2O_3 using halide vapor phase epitaxy. An *m*-plane α-Ga_2O_3/sapphire template with a patterned SiO_2 mask was used as the substrate. The highest lateral growth rate for a radial spoke-wheel patterned mask was obtained when the spoke was perpendicular to the ⟨11$\bar{2}$3⟩ direction. In this case, the lateral-to-vertical growth rate ratio (*L*/*V* ratio), with *L* defined as the rate of increase in the width of an elongated α-Ga_2O_3 island, was as large as 5.8. This ratio was greater than that reported for an *m*-direction stripe mask on *a*-plane α-Ga_2O_3 by a factor of 3.3 and that for an *a*-direction stripe mask on *c*- and *m*-plane α-Ga_2O_3 by a factor of 13. The epitaxial lateral overgrowth (ELO) of α-Ga_2O_3 on a stripe mask (window/mask widths of 2.5 µm/7.5 µm) perpendicular to ⟨11$\bar{2}$3⟩ resulted in the selective nucleation of elongated α-Ga_2O_3 islands with a flat triangular cross-section on the window areas and their coalescence into a compact film. Transmission electron microscopy revealed that the dislocation density in the laterally grown area decreased drastically because the propagation of dislocations in the seed layer was effectively blocked by the mask. We believe these results greatly contribute to the realization of *m*-plane α-Ga_2O_3-based future power devices.

ARTICLE HISTORY
Received 11 February 2025
Revised 25 March 2025
Accepted 25 March 2025

KEYWORDS
α-Ga_2O_3; dislocation; HVPE

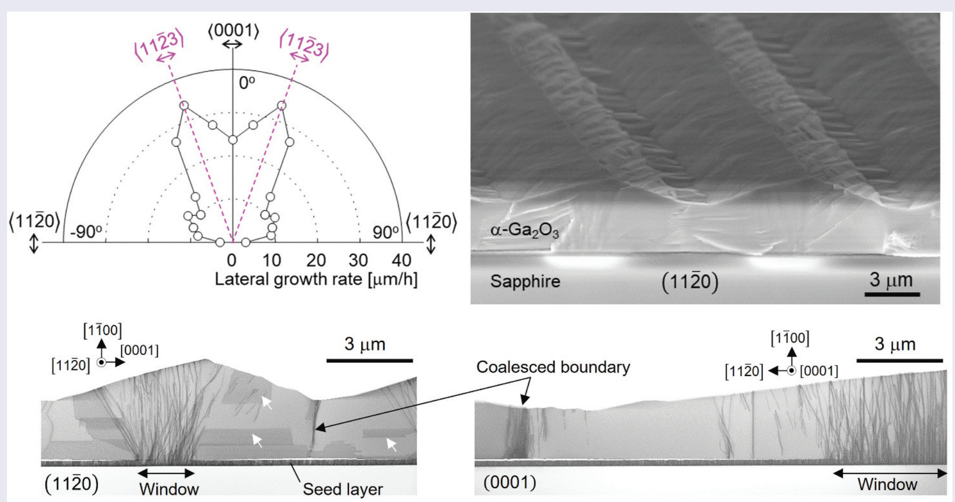

IMPACT STATEMENT
We demonstrated the formation of a compact film of *m*-plane α-Ga_2O_3 by epitaxial lateral growth for the first time and achieved a great reduction in the dislocation density.

Introduction

Ga_2O_3 can crystallize to various polymorphs such as α-, β-, γ-, κ- (ε-), and δ-phases [1–3]. Among them, the β-phase is the most thermodynamically stable under ambient pressure, whereas the others are metastable. Corundum-structured α-Ga_2O_3 is a metastable phase of Ga_2O_3, which is stable up to 500–700°C (a thinner film exhibits higher thermal stability) [4,5]. This material is an ultra-wide-bandgap semiconductor with the highest bandgap energy ($E_g = 5.3$ eV [5,6]) among the Ga_2O_3 polymorphs. In addition, it is possible to prepare solid solutions such as α-$(AlGa)_2O_3$ with other corundum-structured oxides over a wide composition range for band engineering or to impart new functionality [7–9]. Furthermore, isomorphic *p*-type oxides with small lattice mismatches, such as

CONTACT Yuichi Oshima OSHIMA.Yuichi@nims.go.jp Research Center for Electronic and Optical Materials, National Institute for Materials Science (NIMS), 1-1 Namiki, Tsukuba, Ibaraki 305-0044, Japan

© 2025 The Author(s). Published by National Institute for Materials Science in partnership with Taylor & Francis Group.
This is an Open Access article distributed under the terms of the Creative Commons Attribution-NonCommercial License (http://creativecommons.org/licenses/by-nc/4.0/), which permits unrestricted non-commercial use, distribution, and reproduction in any medium, provided the original work is properly cited. The terms on which this article has been published allow the posting of the Accepted Manuscript in a repository by the author(s) or with their consent.

α-$(IrGa)_2O_3$ are available to make a hetero *pn*-junction [10–12]. Therefore, α-Ga_2O_3 is advantageous for realizing high-performance future power devices with high breakdown voltage (V_B) and low energy loss. Indeed, promising device prototypes have been constructed, such as Schottky barrier diodes (SBDs) with a very-low on-resistance of 0.1 mΩcm^2 [13], ampere-class SBDs with a V_B of 1.7 kV, and junction-barrier controlled SBDs with reduced leakage current [14]. In addition, a demonstration of metal-oxide-semiconductor field-effect transistors has been reported [15,16].

α-Ga_2O_3 can be grown through various methods such as mist chemical vapor deposition (CVD) [6], halide vapor phase epitaxy (HVPE) [5,17], molecular beam epitaxy [18,19], metalorganic vapor phase epitaxy [20], and atomic layer deposition [21]. In any methods, isomorphic sapphire is usually used as the substrate, and the crystal planes considered are $c(0001)$, $a(11\bar{2}0)$, $r(\bar{1}012)$, and $m(10\bar{1}0)$. Among these, *m*-plane α-Ga_2O_3 has been reported to exhibit the highest electron mobility [22] and is promising for device applications. However, similar to that of the other planes [23], the observed dislocation density of *m*-plane α-Ga_2O_3 is as high as 10^{10} cm^{-2} [24] because of the large lattice mismatch ($\Delta a/a$ ~ 4.5%, $\Delta c/c$ ~ 3.3%). A theoretical analysis for *m*-plane α-Ga_2O_3 predicts that such a high dislocation density would promote the scattering of free carriers to reduce mobility [25]. Thus, a reduction in dislocation density is essential for achieving increased mobility.

Epitaxial lateral overgrowth (ELO) is an effective method for reducing dislocation density in α-Ga_2O_3 epilayers [23,26–31]. In this method, a dielectric mask, such as SiO_2, with periodically patterned windows is formed on the surface of an α-Ga_2O_3/sapphire template (or sometimes directly on a sapphire substrate), as shown in Figure 1. During the growth process on the masked substrate, α-Ga_2O_3 islands selectively nucleate on the window area, and the islands grow vertically and laterally to coalesce on the mask to form a compact film. As a result of the blocking of the dislocations under the mask, the dislocation density in the laterally grown area of α-Ga_2O_3 drastically

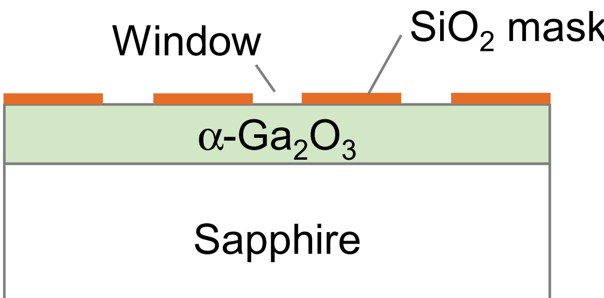

Figure 1. Schematic of the cross-section of an *m*-plane α-Ga_2O_3/sapphire template with a patterned mask.

decreases to 10^7 cm^{-2}, whereas the dislocation density in the window area remains high because the dislocations propagate directly into regrown α-Ga_2O_3 through the window. The successful formation of an α-Ga_2O_3 compact film as a result of island coalescence has been reported on the *c*- [23,26,27,30], *a*- [28], and *r*-planes [29], but not yet on the *m*-plane. To clarify the advantage/disadvantage regarding the choice of substrate plane, let us briefly summarize our past results of ELO on *c*- and *r*-planes by HVPE. The ELO on the *c*-plane requires thick film growth to achieve a coalesced compact film owing to the slow lateral growth rate of *a*- and *m*-plane [23,26,27], while growth conditions are well investigated and very fast growth is possible [32]. Regarding the ELO on the *r*-plane, a compact film can easily be grown because a large lateral growth rate is possible when the stripe mask is aligned along the *a*-axis. In addition, the resulting dislocation density can be much lower than the *c*-plane case because dislocations propagated through the window are overgrown by the α-Ga_2O_3 stripe nucleated on the adjacent window. However, the formation of twin boundaries is problematic [29].

An effective method for decreasing the fraction of the high-dislocation-density area on the windows in an ELO film is the use of a mask with a small fill factor (small window and wide mask) [26]. However, the smaller the fill factor, the longer is the growth time required to achieve island coalescence. It is important to reduce the growth time and film thickness to suppress the cracking or bowing of an epiwafer owing to thermal stress and to decrease the production cost. Accordingly, the lateral-to-vertical growth rate ratio (L/V ratio) of α-Ga_2O_3 islands should be as high as possible. In general, the L/V ratio depends on the crystal orientation and growth conditions. Thus, it is necessary to investigate the influence of crystal orientation on the L/V ratio. Jinno et al. performed the ELO of α-Ga_2O_3 by mist-CVD on *c*-, *m*-, and *a*-plane sapphire with stripe masks oriented in the *a*-, *a*-, and *m*-directions, respectively, to compare the L/V ratios [28]. The L/V ratio for the *a*-plane case was ~ 0.87, whereas those for the *m*- and *c*-plane cases were approximately 1/4 of that for the *a*-plane case. They did not report the coalescence of α-Ga_2O_3 islands on the *m*-plane, possibly because of the low L/V ratio.

In this study, we investigated the in-plane orientation dependence of the lateral growth rate of α-Ga_2O_3 on an *m*-plane substrate. We performed the ELO of α-Ga_2O_3 using a stripe mask pattern along the most suitable direction to efficiently achieve a coalesced compact film with a reduced dislocation density.

Experimental methods

α-Ga_2O_3 was grown in a laboratory-made HVPE reactor at 520°C under atmospheric pressure using O_2

(>99.99995% pure) and GaCl as the precursors. GaCl was synthesized upstream in the reactor through the chemical reaction between metal Ga (>99.99999% pure) and HCl gas (>99.999% pure) at 570°C. The supply partial pressures of $GaCl/O_2$ were 50 Pa/0.2 kPa for the seed layer and 63 Pa/1.0 kPa for ELO. In addition to the growth precursors, HCl gas was directly supplied to the growth zone to suppress parasitic reactions [32]. The partial pressure of HCl was 25 Pa for the seed layer and 188 Pa for ELO. N_2 (dew point <−110°C) was used as the carrier gas. The growth conditions of a small growth rate (~0.6 μm/h) for the seed layer were chosen to enable the nucleation of phase-pure α-Ga_2O_3 on *m*-plane sapphire. The growth conditions of larger growth rate were used for ELO since the ELO process is homoepitaxy on the seed layer, and it is easier to secure the phase-purity. Note that these are not optimized growth conditions to achieve a large lateral growth rate, which should be the focus of future studies.

Figure 1 shows a schematic of the cross-section of the α-Ga_2O_3/sapphire template used for ELO. The seed layer (thickness: 0.3 μm) was grown on an *m*-plane sapphire substrate by HVPE. The mask was SiO_2 (thickness: 40 nm) deposited by RF sputtering and patterned using conventional photolithography. Two mask patterns were used. One was a radial spoke-wheel pattern of rectangular windows ($5 \times 160\ \mu m^2$) aligned with a 10° step. The other was a striped pattern with window and mask widths of 2.5 and 7.5 μm, respectively. The HVPE growth time was 30 min for the spoke-wheel pattern and 15–60 min for the stripe pattern.

Scanning electron microscopy (SEM) was performed using SU8230 (Hitachi, Japan) on the grown samples to observe the morphology and determine the dimensions of the elongated α-Ga_2O_3 islands. The crystal orientation of ELO a-Ga_2O_3 was analyzed by X-ray pole figure measurements using X'pert PRO MRD (Panalytical, Netherlands). The crystal orientation of ELO α-Ga_2O_3 was analyzed by X-ray pole figure measurements. The behavior of the dislocations in ELO a-Ga_2O_3 was investigated using bright-field plan-view and cross-sectional transmission electron microscopy (TEM) using JEM-2100M (JEOL, Japan). The TEM samples were cut by a focused ion beam (FIB) with a thickness of ~200 nm.

Results and discussion

Figure 2(a) shows an X-ray 2θ-ω scan profile of the seed layer. Figure 2(b) shows a magnified spectrum of Figure 2(a) around the peaks. Only the $30\bar{3}0$ diffraction peaks from α-Ga_2O_3 and sapphire were detected. Figure 2(c) shows the ϕ-scan profile of the $11\bar{2}0$ diffraction peak measured with a skew-symmetric geometry. The peaks were observed only at two-fold symmetric positions, which is expected for single-crystalline *m*-plane α-Ga_2O_3. Thus, the seed layer was confirmed to be a phase-pure epitaxial film of *m*-plane α-Ga_2O_3.

Figure 3(a) shows a plan-view SEM image of the sample grown on the spoke-wheel pattern. An elongated α-Ga_2O_3 island grew selectively in each window. The island width was strongly dependent on the spoke direction. In addition, the unintentional formation of hexagonal grains of κ-Ga_2O_3 was observed [23,33]. The seed layer was flat, and the phase purity was confirmed through XRD. Therefore, the κ-Ga_2O_3 grains likely nucleated during the ELO stage. Similar unintentional nucleation of κ-Ga_2O_3 grains was also reported for the ELO of *c*-plane α-Ga_2O_3 by HVPE at the mask edge when the growth-driving force was too high [23]. If the nucleation mechanism of the κ-Ga_2O_3 grains in this study is similar to that reported in the *c*-plane case, slower growth (at least until the mask edge is completely covered by laterally grown α-Ga_2O_3) should be effective in suppressing unintentional nucleation.

In general, precursors adsorbed on the mask can diffuse to reach the window region and contribute to the growth if the distance is less than the diffusion length and the growth is in the mass-transport-limited regime. Therefore, in principle, the island width should be broader when going away from the wheel center because the mask width between the windows increases. However, in reality, such variation in the island width was not observed in Figure 3(a). We speculate that the diffusion length at the low growth temperature of 520°C was much shorter than the window width, and therefore the contribution of adsorbed precursors on the mask was likely to be limited.

Figure 3(b) shows a polar plot of the lateral growth rate calculated from the widths of the elongated α-Ga_2O_3 islands. The spoke direction corresponds to that in Figure 3(a). The crystallographic orientations displayed around the graph are in the lateral growth direction perpendicular to the spoke direction. Lateral growth proceeds on both sides of a window in opposite directions—[0001] and $[000\bar{1}]$ in the case of the $\langle 11\bar{2}0\rangle$-oriented window, for example. Notably, these two directions are not necessarily crystallographically equivalent. Accordingly, the lateral growth rates in two opposite directions should be calculated separately. However, in this study, it was not possible to determine the window-edge positions from the plan-view SEM images. Therefore, we define lateral growth rate L as the rate of increase in the width of an elongated α-Ga_2O_3 island, that is, $L \equiv (W–D)/t$, where W is the width of the elongated α-Ga_2O_3 island, D is the window width, and t is the growth time. This

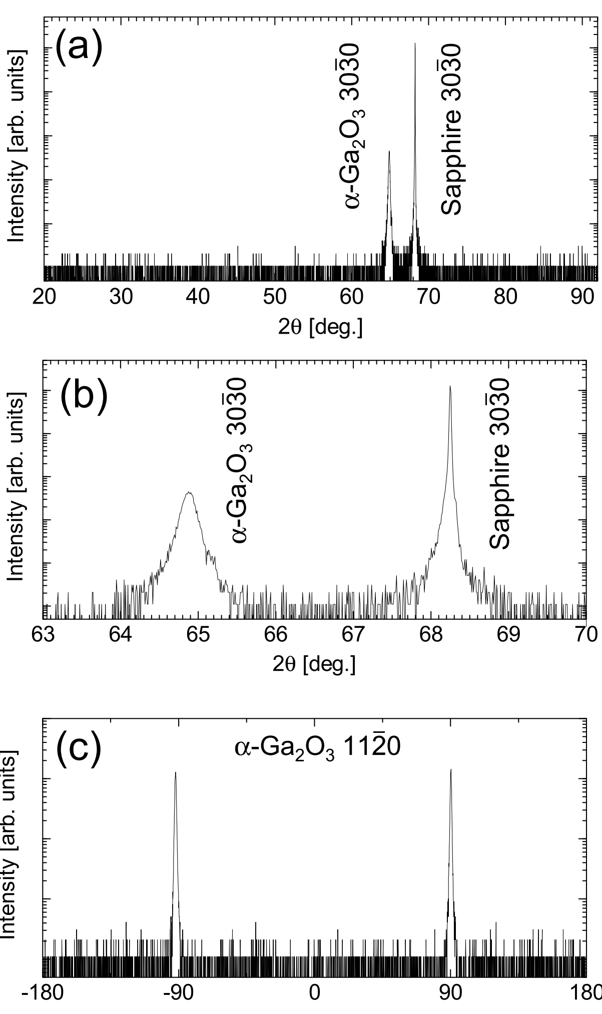

Figure 2. X-ray diffraction patterns of an *m*-plane α-Ga_2O_3 /sapphire template. (a) Out-of-plane 2θ-ω scan profile; (b) magnification at 63°–70°, and (c) skew-symmetric ϕ scan profile of the 11$\bar{2}$0 diffraction.

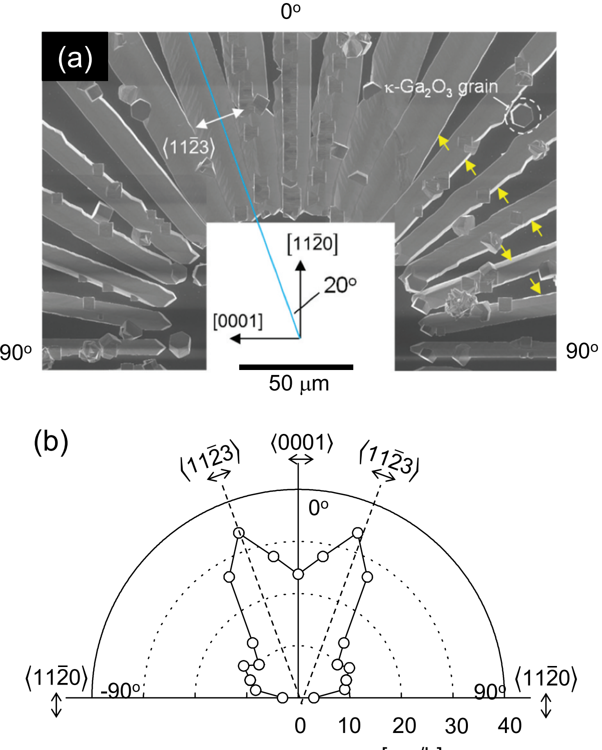

Figure 3. (a) Plan-view SEM image of the sample grown on the radial spoke-wheel pattern. (b) Polar plot of the lateral growth rate as a function of the spoke direction.

definition is useful for determining the optimal window direction for efficient coalescence.

The polar plot shows that the lateral growth rate was the highest when the spoke direction was rotated from the *a*-direction (0°) toward the *c*-direction (±90°) by 20°. In this case, the lateral growth direction was $\langle 11\bar{2}3\rangle$. Growth rate *L* along $\langle 11\bar{2}3\rangle$ was 34 µm/h, which was approximately 11 times greater than that along $\langle 11\bar{2}0\rangle$ (*c*-direction spoke), along which *L* was the lowest. Note that *L* sharply dropped when the spoke direction angle was over ± 30°, and *L* was minimum at ± 90°. The sharp decrease in *L* might be attributed to the formation of side facets. Inclined side facets are visible in Figure 3(a), which are indicated by yellow arrows (only on the right side of the image). At ± 90°, the side wall was a vertical *a*-plane facet. There are growth rate dips at ± 90°, ±50°, and 0°, indicating the formation of specific stable planes. The ± 90°-dips can be attributed to the formation of the *a*-plane side facets. The ± 50°-dips can be attributed to the formation of *r*-plane side facets because these directions are close to the intersection lines of *m*-and *r*-planes (±43.4°), and the inclination of the side facets was approximately 66°, which was close to the angle between the *m*- and *r*-planes (65.1°). At 0°, the elongated α-Ga_2O_3 island consisted of only inclined top planes without side facets. The top planes should be $(\bar{1}101)$ (S-plane) and $(1\bar{1}01)$ (see next paragraph for details regarding the determination of these indices). The relatively large *L* at 0° indicates that $(\bar{1}101)$ and $(1\bar{1}01)$ are less stable than the side facets at ± 90° and ± 50° under the growth conditions used for the present work, but stable enough to make the 0°-dip. When the spoke angle was deviated from 0°, the atomic step density on the top surface should increase to give an even greater *L*. However, when the deviation reached approximately ± 30°, the *L* should be limited by the formation of the side facets. This trade-off may be the reason why *L* was maximum at ± 20°.

Figure 4(a–f) shows the SEM images depicting the time evolution of the growth process on the stripe mask aligned so that the lateral growth direction was $\langle 11\bar{2}3\rangle$. Note that the cross-sectional observation was performed along the *a*-direction, which was not parallel to the stripe, because the *a*-plane cross-section was exposed by cleaving the sample along the *c*-direction. At a growth time of 15 min (Figure 4(a,d)), the α-Ga_2O_3 stripes with triangular cross-sections were still isolated. The *L*/*V* ratio was estimated to be ~5.8, which was greater than that reported for the *m*-oriented stripe on *a*-plane α-Ga_2O_3 and the *a*-oriented stripe on *c*- and *m*-plane α-Ga_2O_3 by a factor of 3.3 and 13,

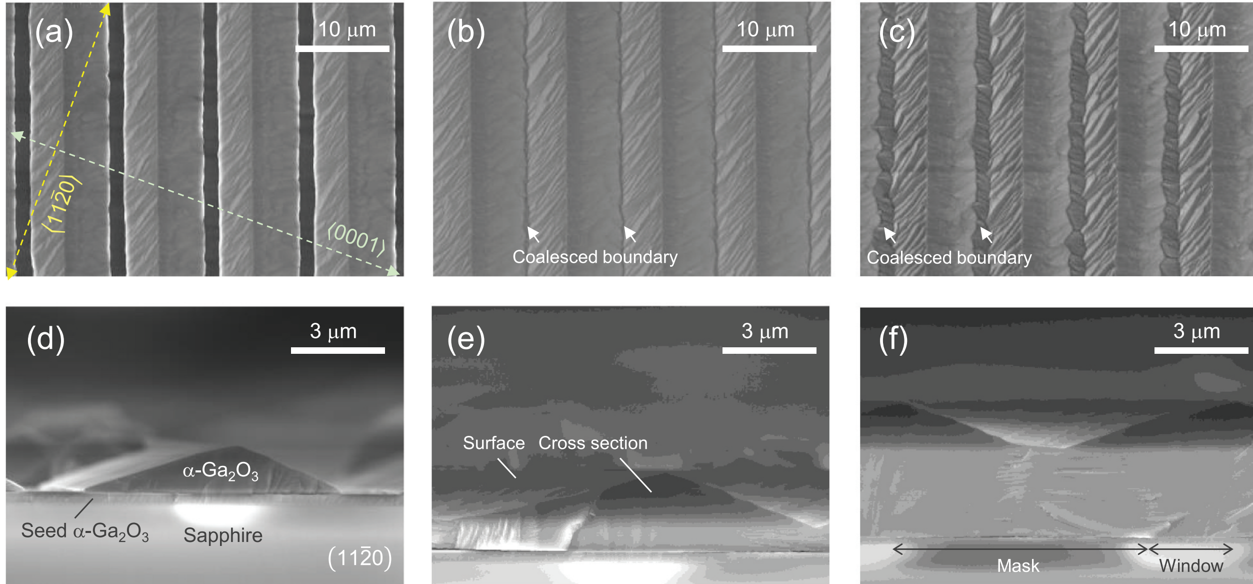

Figure 4. Plan-view and cross-sectional SEM images of the ELO samples at different growth stages of (a), (d) 15 min, (b), (e) 30 min, and (c), (f) 60 min.

respectively [28]. The reported L/V ratios were doubled for comparison. At 30 min (Figure 4(b,e)), a compact film was formed because of island coalescence. At 60 min (Figure 4(c,f)), the valley-to-top thickness ratio was smaller than that at 15 min, indicating that the film was approaching flattening. The top surfaces were inclined from the m-plane by approximately 18°. The angles were close to the inclination angles of (1$\bar{1}$01) and ($\bar{1}$101) from the m-plane (17.8°). In Figure 4, the left/right side slopes of an elongated α-Ga_2O_3 island correspond to (1$\bar{1}$01) and ($\bar{1}$101), respectively. The morphologies of both slopes were different (left slope was rougher) probably because these planes are crystalographically different since α-Ga_2O_3 is not hexagonal but trigonal.

Figure 5 shows the X-ray pole figure of the 60-min-growth sample shown in Figure 4(c,f). The 2θ/ω angles were set to detect the 10$\bar{1}$4 diffraction. The peaks appear only at the positions expected for single-crystalline m-plane α-Ga_2O_3, and no misoriented α-Ga_2O_3 domains are detected.

Figure 6(a) shows the bird's-eye-view SEM image of the 60-min-growth sample. Figure 6(b) shows the plan-view TEM image of the same sample. The sample was horizontally cut by FIB at a depth close to the surface of the coalesced boundary. A magnified image on the window region is also shown as the inset. Dislocations are visible as dots or line segments with lengths dependent on the inclination angles. In Figure 6(b), a high-dislocation-density area elongated along the stripe direction is visible around the center with a width of a few micrometers, which was comparable to the window width. In addition, narrower high-dislocation-density areas are visible on both sides of the image with a spacing of ~10 μm, which is the period of the stripe mask.

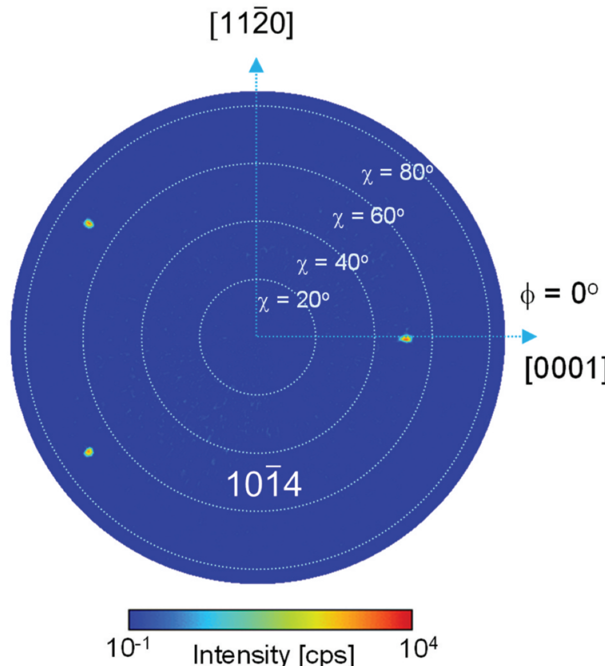

Figure 5. X-ray pole figure of the ELO sample grown on the stripe mask pattern for 60 min. The 2θ/ω angles were set to detect the 10$\bar{1}$4 diffraction.

Figure 6(c,d) show the cross-sectional TEM images in the a- and c-directions, respectively. The TEM images revealed that the high-dislocation-density areas observed in Figure 6(b) was due to the propagation of dislocations into regrown α-Ga_2O_3 from the seed layer through the windows and dislocation formation at the coalesced boundaries, as observed on other planes [23,26–29]. A part of the dislocations propagated through the window inclined to follow the inclined surface. As a result, the dislocation density at the top surface above the window was lower than

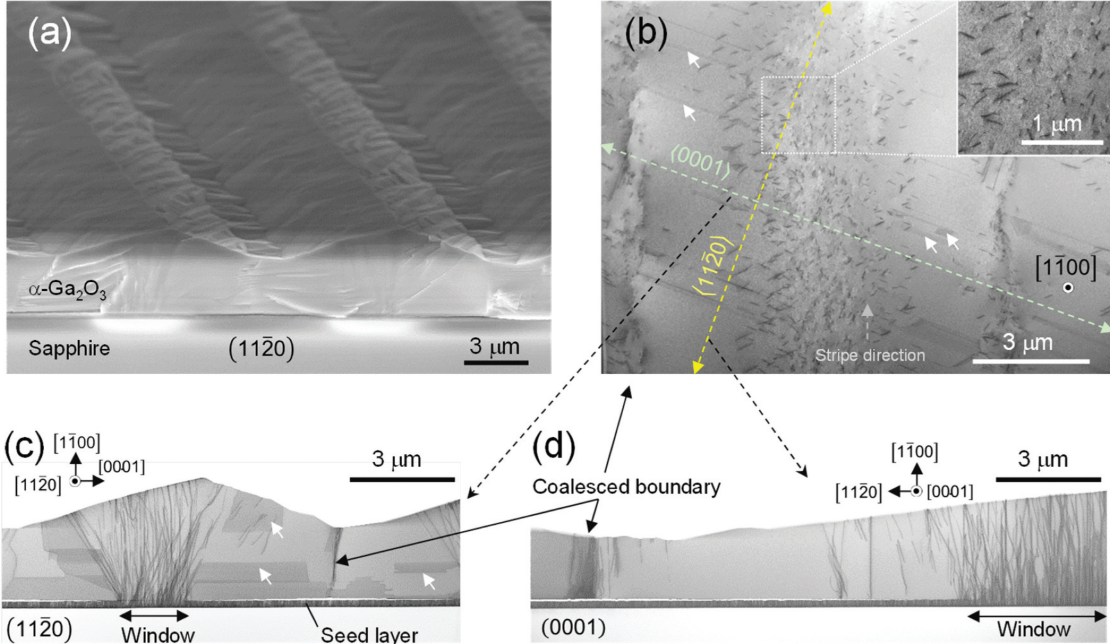

Figure 6. SEM and TEM images of the ELO sample grown on the stripe mask pattern for 60 min. (a) Bird's's eye-view SEM image, (b) plan-view TEM image with a magnified image on the window region as the inset, (c) and (d) cross-sectional TEM images viewed from *a*- and *c*-axes, respectively. Some of the band-like contrasts are indicated by white arrows in (b) and (c).

that in the seed layer. A part of the propagated dislocations did not bend. The reason for the different behavior is not clear at present, but maybe the dislocation character was different. The dislocation density at the coalesced front looks comparable to that on the window, and the influence on the device performance should be significant. Countermeasures such as facet-controlled thick film growth [34] should be effective to decrease the residual dislocations. In the laterally grown area, the dislocation density was drastically reduced because the dislocations in the seed layer were blocked by the mask. In addition to the dislocation contrast, a band-like contrast elongated along the *c*-direction is visible in Figure 6(c), but not in Figure 6(d). A band-like contrast was also visible in the plan-view image (Figure 6(b)) although the width was small. Accordingly, it is likely that the band-like contrast occurred owing to planar defects, such as stacking faults, which were slightly rotated from the *a*-plane around the *c*-axis. Further studies are necessary to clarify the origin of the band-like contrast by high-resolution TEM and to improve the growth conditions to suppress it.

Summary

In this study, we demonstrated the ELO of α-Ga_2O_3 on the *m*-plane using HVPE. The anisotropy of the lateral growth rate was investigated using a radial-spoke-patterned mask, and the highest lateral growth rate was obtained along the $\langle 11\bar{2}3 \rangle$ direction. Lateral growth rate L along $\langle 11\bar{2}3 \rangle$ was 34 μm/h, which was approximately 11 times higher than that along $\langle 11\bar{2}0 \rangle$, along which it was slowest. In the $\langle 11\bar{2}3 \rangle$ case, the L/V ratio was 5.8, which was greater than the reported values for *a*-plane α-Ga_2O_3 with an *m*-direction stripe mask and *m*- and *c*-plane α-Ga_2O_3 with an *a*-direction stripe mask by a factor of 3.3 and 13, respectively. ELO was performed using the stripe mask pattern with window/mask widths of 2.5/7.5 μm aligned to give the highest lateral growth rate, and a compact film was achieved in <30 min. Plan-view and cross-sectional TEM images of the compact film revealed a significant reduction in the dislocation density in the laterally grown area although the dislocations propagated in the window area and were newly formed at the coalesced boundary. Planar defects were also observed in addition to dislocations. Thus, we believe that this technique will significantly contribute to the development of high-performance α-Ga_2O_3-based devices although the growth conditions require further improvement.

Acknowledgments

This work was supported by the "Advanced Research Infrastructure for Materials and Nanotechnology in Japan (ARIM)" initiative of the Ministry of Education, Culture, Sports, Science, and Technology (MEXT) under Proposal Number JPMXP1224NM5455.

Disclosure statement

No potential conflict of interest was reported by the author(s).

Funding

This study was supported by the Innovative Science and Technology Initiative for Security [Grant Number JPJ004596], ATLA, Japan.

ORCID

Yuichi Oshima http://orcid.org/0000-0001-8293-4891
Takashi Shinohe http://orcid.org/0009-0000-5559-1432

References

[1] Roy R, Hill VG, Osborn EF. Polymorphism of Ga_2O_3 and the system Ga_2O_3 —H_2O. J Am Chem Soc. 1952;74(3):719–722. doi: 10.1021/ja01123a039
[2] Playford HY, Hannon AC, Barney ER, et al. Structures of uncharacterised polymorphs of gallium oxide from total neutron diffraction. Chem - A Eur J. 2013;19(8):2803–2813. doi: 10.1002/chem.201203359
[3] Cora I, Mezzadri F, Boschi F, et al. The real structure of ε-Ga_2O_3 and its relation to κ-phase. CrystEngcomm. 2017;19(11):1509–1516. doi: 10.1039/C7CE00123A
[4] Jinno R, Kaneko K, Fujita S. Thermal stability of α-Ga_2O_3 films grown on *c*-plane sapphire substrates via mist-CVD. AIP Adv. 2021;10(11):115013. doi: 10.1063/5.0020464
[5] Oshima Y, Víllora EG, Shimamura K. Halide vapor phase epitaxy of twin-free α-Ga_2O_3 on sapphire (0001) substrates. Appl Phys Express. 2015;8(5):055501. doi: 10.7567/APEX.8.055501
[6] Shinohara D, Fujita S. Heteroepitaxy of corundum-structured α-Ga_2O_3 thin films on α-Al_2O_3 substrates by ultrasonic mist chemical vapor deposition. Jpn J Appl Phys. 2008;47(9R):7311–7313. doi: 10.1143/JJAP.47.7311
[7] Ito H, Kaneko K, Fujita S. Growth and band gap control of corundum-structured α-$(AlGa)_2O_3$ thin films on sapphire by spray-assisted mist chemical vapor deposition. Jpn J Appl Phys. 2012;51(10R):100207. doi: 10.7567/JJAP.51.100207
[8] Kaneko K, Nomura T, Kakeya I, et al. Fabrication of highly crystalline corundum-structured α-$(Ga_{1-x}Fe_x)_2O_3$ alloy thin films on sapphire substrates. Appl Phys Express. 2009;2:075501. doi: 10.1143/APEX.2.075501
[9] Fujita S, Kaneko K. Epitaxial growth of corundum-structured wide band gap III-oxide semiconductor thin films. J Cryst Growth. 2014;401:588–592. doi: 10.1016/j.jcrysgro.2014.02.032
[10] Kan S, Takemoto S, Kaneko K, et al. Electrical properties of α-Ir_2O_3/α-Ga_2O_3 pn heterojunction diode and band alignment of the heterostructure. Appl Phys Lett. 2018;113(21):212104. doi: 10.1063/1.5054054
[11] Kaneko K, Fujita S, Hitora T. A power device material of corundum-structured α-Ga_2O_3 fabricated by MIST EPITAXY® technique. Jpn J Appl Phys. 2018;57(2S2):02CB18. doi: 10.7567/JJAP.57.02CB18
[12] Kaneko K, Masuda Y, Kan S, et al. Ultra-wide bandgap corundum-structured p-type α-$(Ir,Ga)_2O_3$ alloys for α-Ga_2O_3 electronics. Appl Phys Lett. 2021;118(10):102104. doi: 10.1063/5.0027297
[13] Oda M, Tokuda R, Kambara H, et al. Schottky barrier diodes of corundum-structured gallium oxide showing on-resistance of 0.1 mω·cm^2 grown by MIST EPITAXY®. Appl Phys Express. 2016;9(2):021101. doi: 10.7567/APEX.9.021101
[14] Shinohe T. Innovative power electronics for all users - progress in ultra-wide bandgap α-Ga_2O_3. In: Proceedings of the 2024 IEEE International Meeting for Future of Electron Devices; Kansai; 2024. p. 1–4.
[15] Shinohe T. Development of α-Ga_2O_3 power devices. In: Proceedings of the 2022 International Power Electronics Conference (IPEC-Himeji 2022-ECCE Asia); Himeji, Japan; 2022. p. 627–631.
[16] Jeong YJ, Park JH, Yeom MJ, et al. Heteroepitaxial α-Ga_2O_3 MOSFETs with a 2.3 kV breakdown voltage grown by halide vapor-phase epitaxy. Appl Phys Express. 2022;15(7):074001. doi: 10.35848/1882-0786/ac7431
[17] Jeon DW, Son H, Hwang J, et al. Electrical properties, structural properties, and deep trap spectra of thin α-Ga_2O_3 films grown by halide vapor phase epitaxy on basal plane sapphire substrates. APL Mater. 2018;6(12):121110. doi: 10.1063/1.5075718
[18] Cheng Z, Hanke M, Vogt P, et al. Phase formation and strain relaxation of Ga_2O_3 on *c*-plane and *a*-plane sapphire substrates as studied by synchrotron-based x-ray diffraction. Appl Phys Lett. 2017;111(16):162104. doi: 10.1063/1.4998804
[19] Jinno R, Chang CS, Onuma T, et al. Crystal orientation dictated epitaxy of ultrawide-bandgap 5.4-to 8.6-eV α-$(AlGa)_2O_3$ on m-plane sapphire. Sci Adv. 2021;7(2):eabd5891. doi: 10.1126/sciadv.abd5891
[20] Bhuiyan AFMAU, Feng Z, Huang HL, et al. Metalorganic chemical vapor deposition of α-Ga_2O_3 and α-$(Al_xGa1-x)_2O_3$ thin films on *m*-plane sapphire substrates. APL Mater. 2021;9(10):101109. doi: 10.1063/5.0065087
[21] Roberts JW, Jarman JC, Johnstone DN, et al. α-Ga_2O_3 grown by low temperature atomic layer deposition on sapphire. J Cryst Growth. 2018;487:23–27.
[22] Akaiwa K, Ota K, Sekiyama T, et al. Electrical properties of Sn-doped α-Ga_2O_3 films on *m*-plane sapphire substrates grown by mist chemical vapor deposition. Phys Status Solidi A. 2020;217(3):1900632. doi: 10.1002/pssa.201900632
[23] Oshima Y, Kawara K, Shinohe T, et al. Epitaxial lateral overgrowth of α-Ga_2O_3 by halide vapor phase epitaxy. APL Mater. 2019;7(2):022503. doi: 10.1063/1.5051058
[24] Takane H, Konishi S, Hayasaka Y, et al. Structural characterization of threading dislocation in α-Ga_2O_3 thin films on *c*- and *m*-plane sapphire substrates. J Appl Phys. 2024;136(2):025105. doi: 10.1063/5.0206863
[25] Takane H, Izumi H, Hojo H, et al. Effect of dislocations and impurities on carrier transport in α-Ga_2O_3 on *m*-plane sapphire substrate. J Mater Res. 2023;38(10):2645–2654. doi: 10.1557/s43578-023-01015-8
[26] Oshima Y, Kawara K, Oshima T, et al. Phase-controlled epitaxial lateral overgrowth of α-Ga_2O_3 by halide vapor phase epitaxy. Jpn J Appl Phys. 2020;59(2):025512. doi: 10.35848/1347-4065/ab6faf
[27] Kawara K, Oshima Y, Okigawa M, et al. Elimination of threading dislocations in α-Ga_2O_3 by double-layered epitaxial lateral overgrowth. Appl Phys Express. 2020;13(7):075507. doi: 10.35848/1882-0786/ab9fc5
[28] Jinno R, Yoshimura N, Kaneko K, et al. Enhancement of epitaxial lateral overgrowth in the mist chemical

vapor deposition of α-Ga_2O_3 by using a-plane sapphire substrate. Jpn J Appl Phys. 2019;58(12):120912. doi: 10.7567/1347-4065/ab55c6

[29] Oshima Y. Epitaxial lateral overgrowth of r-plane α-Ga_2O_3 with stripe masks along ⟨1¯21¯⟩. J Appl Phys. 2021;130(17):175304. doi: 10.1063/5.0068097

[30] Son H, Choi Y, Ha J, et al. Crystal quality improvement of α-Ga_2O_3 growth on stripe patterned template via epitaxial lateral overgrowth. Cryst Growth Des. 2019;19(9):5105–5110. doi: 10.1021/acs.cgd.9b00454

[31] Zhang Y, Wang Z, Kuang Y, et al. Dislocation dynamics in α-Ga_2O_3 micropillars from selective-area epitaxy to epitaxial lateral overgrowth. Appl Phys Lett. 2022;120(12):121601. doi: 10.1063/5.0085367

[32] Oshima Y, Kawara K, Oshima T, et al. Rapid growth of α-Ga_2O_3 by HCl-boosted halide vapor phase epitaxy and effect of precursor supply conditions on crystal properties. Semicond Sci Technol. 2020;35(5):055022. doi: 10.1088/1361-6641/ab7843

[33] Oshima Y, Kawara K, Oshima T, et al. In-plane orientation control of (001) κ-Ga_2O_3 by epitaxial lateral overgrowth through a geometrical natural selection mechanism. Jpn J Appl Phys. 2020;59(11):115501. doi: 10.35848/1347-4065/abbc57

[34] Oshima Y, Ando H, Shinohe T. Reduction of dislocation density in α-Ga_2O_3 epilayers via rapid growth at low temperatures by halide vapor phase epitaxy. Appl Phys Express. 2023;16(6):065501. doi: 10.35848/1882-0786/acddca